

3XMM J181923.7–170616: AN X-RAY BINARY WITH A 408 S PULSAR

HAO QIU,¹ PING ZHOU,^{1,2,3} WENFEI YU,⁴ XIANGDONG LI,^{1,3} AND XIAOJIE XU^{1,3}¹*School of Astronomy and Space Science, Nanjing University, 163 Xianlin Avenue, Nanjing, 210023, China*²*Anton Pannekoek Institute for Astronomy, University of Amsterdam, Science Park 904, 1098 XH Amsterdam, The Netherlands**³*Key Laboratory of Modern Astronomy and Astrophysics, Nanjing University, Ministry of Education, China*⁴*Key Laboratory for Research in Galaxies and Cosmology, Shanghai Astronomical Observatory, Chinese Academy of Sciences, 80 Nandan Road, Shanghai 200030, China*

ABSTRACT

We carry out a dedicated study of 3XMM J181923.7–170616 with an approximate pulsation period of 400 s using the *XMM-Newton* and *Swift* observations spanning across nine years. We have refined the period of the source to 407.904(7) s (at epoch MJD 57142) and determined a period derivative limit of $\dot{P} \leq 5.9 \pm 5.4 \times 10^{-9} \text{ s s}^{-1}$ (1σ). The source radiates hard, persistent X-ray emission during the observation epochs, which is best described by an absorbed *power-law* model ($\Gamma \sim 0.2\text{--}0.8$) plus faint Fe lines at 6.4 keV and 6.7 keV. The X-ray flux revealed a variation within a factor of 2, along with a spectral hardening as the flux increased. The pulse shape is sinusoid-like and the spectral properties of different phases do not present significant variation. The absorption N_{H} ($\sim 1.3 \times 10^{22} \text{ cm}^{-2}$) is similar to the total Galactic hydrogen column density along the direction, indicating that it is a distant source. A search for the counterpart in optical and near-infrared surveys reveals a low mass K-type giant, while the existence of a Galactic OB supergiant is excluded. A symbiotic X-ray binary is the favored nature of 3XMM J181923.7–170616 and can essentially explain the low luminosity of $2.78 \times 10^{34} d_{10}^2 \text{ erg s}^{-1}$, slow pulsation, hard X-ray spectrum, and possible K3 III companion. An alternative explanation of the source is a persistent Be/X-ray binary with a companion star no earlier than B3-type.

Keywords: X-rays: Binaries — binaries: symbiotic — stars: individual (3XMM J181923.7–170616 =Swift J1819.2–1706)

* p.zhou@uva.nl

1. INTRODUCTION

X-ray Binaries (XRBs) are binary systems in which a compact object (such as a neutron star or a black hole) is accreting from a companion star, contributing a significant amount of X-ray radiation in one galaxy. XRBs are divided into two categories according to the mass of the companion star. A binary with a massive companion ($> 8M_{\odot}$) is called a high mass X-ray binary (HMXB), while those with smaller companions ($< 1M_{\odot}$) are classified as low mass X-ray binaries (LMXBs).

LMXBs are usually transient sources, in their quiescent states the X-ray luminosities can be down to $10^{32} \text{ erg s}^{-1}$ in the soft X-ray band, and they can turn to be very luminous during the outbursts (up to $10^{38} \text{ erg s}^{-1}$, see Reig 2011 for a recent review). HMXB systems are mainly subdivided into Be/X-ray Binaries (BeXBs) and supergiant X-ray binaries (SGXBs). BeXBs contain a neutron star (NS) orbiting a Be star (Negueruela 1998). Most of them display two types of outbursts (Type I and II) during which the luminosity is increased significantly ($\Delta L_X \sim 100\text{-}1000$). With the improved sensibilities of X/ γ -ray telescopes, the above picture of XRBs has been enriched with emerging subclasses. Symbiotic X-ray binaries (SyXBs) are a new subclass of LMXBs containing an X-ray luminous NS and a late type giant companion. Our current knowledge of SyXBs comes from about 10 SyXBs or potential candidates, which manifest long orbital and spin periods ($> 100 \text{ s}$) and a relatively low X-ray luminosity ($10^{32}\text{-}10^{36} \text{ erg s}^{-1}$; Lü et al. 2012). The long spin period and weak X-ray emission are also typical for the persistent BeXBs, in which the NS is suggested to be far from the Be star and accreting material from the low-density regions of the Be star’s wind (Reig & Roche 1999).

During the past two decades, the X-ray space telescopes *XMM-Newton* and *Chandra* have detected numerous serendipitous X-ray sources thanks to their high sensibilities. Their catalogues record X-ray objects with a variety of populations and provide rich resources for the exploration of new XRBs.

3XMM J181923.7–170616 is an X-ray source recorded in the third XMM serendipitous source catalogue Data Release 5 (3XMM-DR5; Rosen et al. 2016). It was identified as a slow X-ray pulsar candidate with a period of 400 s in a study of the 3XMM-DR4 using the machine learning method (Farrell et al. 2015). We performed periodicity search of a selected sample of sources in 3XMM-DR5 and also noticed the clear periodicity of the source at $\sim 408 \text{ s}$.

To uncover the nature of 3XMM J181923.7–170616, we carried out a dedicated analysis of 3XMM J181923.7–170616 using 12 new *Swift* observations in addition to the *XMM-Newton* observations. In Section 2 we describe the X-ray observations used in this study. Our timing and spectral analysis with the *XMM-Newton* and *Swift*-XRT observations are presented in Section 3. The search for the counterpart and our discussion related to the nature are included in Section 4. Section 5 summarizes the results.

2. OBSERVATIONS

2.1. *XMM-Newton*

3XMM J181923.7–170616 was observed in three *XMM-Newton* observations with the European Photon Imaging Camera (EPIC), which contains two MOS cameras (Turner et al. 2001) and a pn camera (Strüder et al. 2001) to detect X-ray photons in the 0.2–10 keV energy range. All of these three observations were originally pointed to an HXMB SAX J1818.6-1703 ($18^{\text{h}}18^{\text{m}}37^{\text{s}}.90$, $-17^{\circ}02'47''.96$, J2000) and detected the serendipitous bright source 3XMM J181923.7–170616 $12'$ away to the south-east. Two observations of the source conducted in 2006 (PI D.M. Smith) and 2010 (PI E. Bozzo)

were recorded in 3XMM-DR5. A third observation (PI S. Drave) was carried out in 2013, it was not included in the 3XMM catalogue. We only use the MOS data of the third observation because 3XMM J181923.7–170616 was beyond the field of view of the pn camera observation. The Reflection Grating Spectrometer (RGS) data of each observation has a cross dispersion of $5'$, in which the source was out of the field. Therefore we do not perform an analysis of the RGS data. The time resolutions of the MOS and pn data are 2.6 s and 73.4 ms, respectively. We removed the time intervals with strong heavy proton flaring by checking the CCD corner light curves. Since the third observation has an unsteady light curve in most of the observation time, we only used the time intervals with flat, low counts rate and did not refer to this observation for precise analysis. The total screened exposures for the MOS1/2 and pn data are 54 ks and 26.7 ks, respectively. XMM Science Analysis System software (SAS, ver 15.0) was used to reproduce the *XMM-Newton* data.

2.2. *Swift*

We found additional data of 3XMM J181923.7–170616 observed with the *Swift* space telescope in the HEASARC¹ data archive. There are 12 observations toward the X-ray point source SWIFT J1819.2-1706 that spatially matches 3XMM J181923.7–170616. We believe that they are the same source because of their spatial coincidence and identical timing and spectral properties (see Section 3).

The *Swift* observations were conducted between April 30 and May 31, 2015. We retrieved the Ultraviolet/Optical Telescope (UVOT) imaging data for the 170-650 nm and X-ray telescope (XRT) data in the 0.2-10 keV energy range. We chose the PC mode of XRT data and processed them using the HEASOFT Calibration Database. UVOT data are not used in this paper, because we did not find a counterpart of the source in the *Swift* UV/Optical image. The XRT CCD time resolution is 2.5 s. The minimum, maximum, and total exposures amongst XRT observations are approximately 1.5 ks, 10.3 ks, and 88.3 ks, respectively.

XSPEC(ver 12.9.0) and XRONOS packages in HEASOFT(ver 6.17), and TEMPO2² (Hobbs et al. 2006; Edwards et al. 2006) were used for timing and spectral analysis of the *XMM-Newton* and *Swift* data. We also used Python software packages (Astropy, Scipy/Numpy and Matplotlib) for data analysis and visualization. Table 1 lists the detailed information (the observation ID, date, exposure, and average count rate) of the X-ray observations.

3. RESULTS

3.1. *Timing Analysis*

The photons of 3XMM J181923.7–170616 are extracted from a circular region with a radius of $30''$ centered at ($18^{\text{h}}19^{\text{m}}23^{\text{s}}.77$, $-17^{\circ}06'15''.25$, J2000). We corrected the photon's arrival time to the barycenter of the solar system before the periodicity search. The power spectral density of the time series in 0.2–10 keV band was calculated with the *powspec* command in the XRONOS package. The upper limits of the calculated frequencies are ~ 0.2 Hz for the MOS and XRT data, and 7 Hz for the pn data. A power density peak is shown at 0.0025 Hz in the *XMM-Newton* and *Swift* power spectra, corresponding to a periodicity of ~ 400 s. We subsequently apply the epoch-folding method (*efsearch*; Leahy 1987), which refines the periodicity to around 408 s. The uncertainty of the period σ_p is estimated with $\sigma_P = 0.71(\chi_r^2 - 1)^{-0.63}\Delta P$, where $\Delta P = P^2/(2T_s)$ is the Fourier resolution for

¹ <http://heasarc.gsfc.nasa.gov/>

² <http://www.atnf.csiro.au/research/pulsar/tempo2/>

an observation duration of T_s and χ_r^2 is the peak theoretical reduced Chi-square in the χ^2 vs. period plot (see Leahy 1987). Table 1 summarizes the 9 groups (3 for MOS1, 3 for MOS2, 2 for pn, and 1 for XRT of *Swift*) of periods. In this process we combine the 12 *Swift* observations taken within two months.

We construct a phase-connection analysis by fitting the time-of-arrivals (TOAs) of the observations to a standard timing model: $\phi(t) = \phi(t_0) + (t - t_0)/P - (t - t_0)^2\dot{P}/(2P^2)$. The TOA of each observation is determined by folding the pulse profile with a period of 407.9091 s. This period with a small uncertainty (0.0025 s) is taken from the epoch-folding result of the *Swift* data (see Table 1). A sinusoid can reproduce each folded pulse profile and is thus used to determine the TOA of each observation. The *Swift* data with the ID of 00033498008 are not used for the phase connection, since the short exposure (1.5 ks; less than 4 periods) is insufficient to provide a reliable TOA.

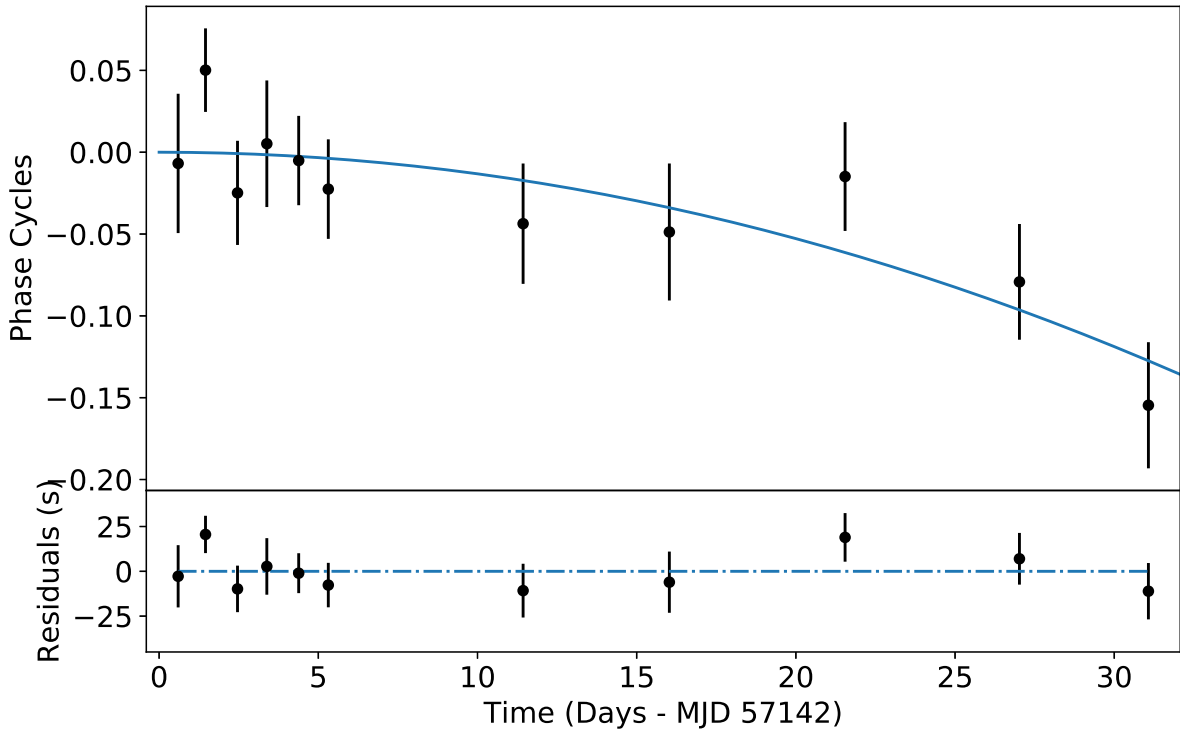


Figure 1. Time/Phase residuals of the 11 XRT TOAs after subtraction of the best-fit quadratic ephemeris model ($P = 407.904$ s at MJD 57142, $\dot{P} = 5.9 \times 10^{-9}$ s s $^{-1}$). The top panel shows the timing residuals subtracting only the contribution of the linear component of the best-fit ephemeris, with the solid line showing the quadratic term. The lower panel gives the time residuals respect to the quadratic ephemeris model.

We started by fitting the first three TOAs to a linear ephemeris and added TOAs one at a time using a quadratic ephemeris. We repeated the fit procedure iteratively using the new solution until the last TOA is added. Each newly added TOA matches to $\lesssim 0.1$ cycles of the predicted phase derived from the previous solution. The best-fit quadratic ephemeris is given by the final phase-fitting procedure: $P = 407.904(7)$ s on MJD 57142 and $\dot{P} = 5.9 \pm 5.4 \times 10^{-9}$ s s $^{-1}$ (1σ uncertainty; rms=10.8 s, $\chi^2/d.o.f = 8.2/8 = 1.03$; see Figure 1.). During the *Swift* observation epoch, the quadratic term contributes -0.06 (-0.01 – -0.24) cycles. We did not fit retroactively back to the

Table 1. Summary of the *XMM-Newton* and *Swift* observations and the timing properties of 3XMM J181923.7–170616

Obs. ID	Obs. Date	Exposure ^a (ks)	Instrument	Count Rate ^b (counts s ⁻¹)	Period ^c (s)
0402470101	2006 Oct 07	13.1/18.2	XMM/MOS1	0.036(2)	408.0(9)
		13.3/18.2	XMM/MOS2	0.037(2)	409(1)
		11.7/18.2	XMM/pn	0.058(4)	408.9(6)
0604820101	2010 Mar 21	28.6/45.6	XMM/MOS1	0.045(2)	407.7(2)
		24.3/45.6	XMM/MOS2	0.042(2)	408.2(2)
		15.0/45.6	XMM/pn	0.108(4)	407.7(2)
0693900101 ^d	2013 Mar 21	12.5/30.7	XMM/MOS1	0.054(3)	406.7(3)
		12.5/30.7	XMM/MOS2	0.054(2)	409.1(4)
00033498001	2015 Apr 30	9.6	Swift/XRT	0.022(1)	407.909(3)
00033498002	2015 May 01	8.6	Swift/XRT	0.026(1)	-
00033498003	2015 May 02	5.0	Swift/XRT	0.027(2)	-
00033498004	2015 May 03	9.8	Swift/XRT	0.026(1)	-
00033498005	2015 May 04	10.3	Swift/XRT	0.022(1)	-
00033498006	2015 May 05	9.0	Swift/XRT	0.019(1)	-
00033498007	2015 May 11	7.3	Swift/XRT	0.024(1)	-
00033498008	2015 May 14	1.5	Swift/XRT	0.024(4)	-
00033498009	2015 May 16	5.5	Swift/XRT	0.018(2)	-
00033498010	2015 May 21	9.0	Swift/XRT	0.026(1)	-
00033498011	2015 May 27	5.2	Swift/XRT	0.019(3)	-
00033498012	2015 May 31	7.5	Swift/XRT	0.019(2)	-

^a For *XMM-Newton* observations we show the flare-screened exposure/the total exposure

^b The count rate in 0.3–10 keV is calculated in the flare-screened time. The 1- σ uncertainty of the last digit is given in the parentheses.

^c The uncertainty (Leahy 1987) of the last one digit is given in parentheses.

^d The observation suffered flarings in most of the observation time, which may cause problematic timing results.

XMM-Newton TOAs, considering that a constant \dot{f} would contribute -37 – -882 cycles between the last *XMM-Newton* TOA and the first *Swift* TOA. The quadratic solution is marginally better than a linear solution ($P = 407.912(2)$; rms=11.5 s, $\chi^2/d.o.f = 9.6/9 = 1.06$).

The background-subtracted pulse profiles of 3XMM J181923.7–170616 in 0.3–10 keV are shown in Figure 2, in which one phase corresponds to a period of 407.904 s. The pulse profile maintains a nearly single-peak shape in 2006, 2010, and 2015, with small variation in the profile.

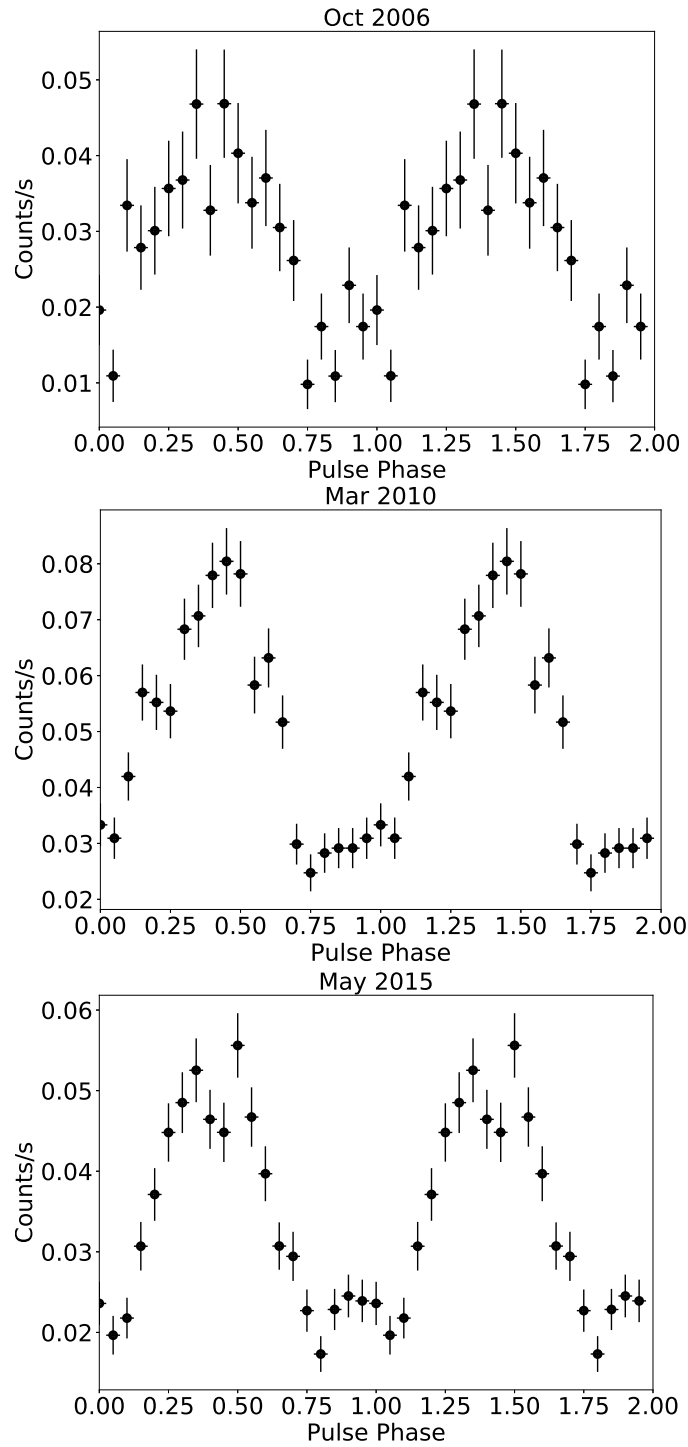


Figure 2. Pulse profiles of 3XMM J181923.7–170616 in October 2006, March 2010 and May 2015.

3.2. Spectral Analysis

The *XMM-Newton* and *Swift* spectra are extracted from a circular region centered at 3XMM J181923.7–170616 with a radius of $30''$. The local background is selected from an annulus region centered at the point source with an inner radius of $55''$ and an outer radius of $120''$.

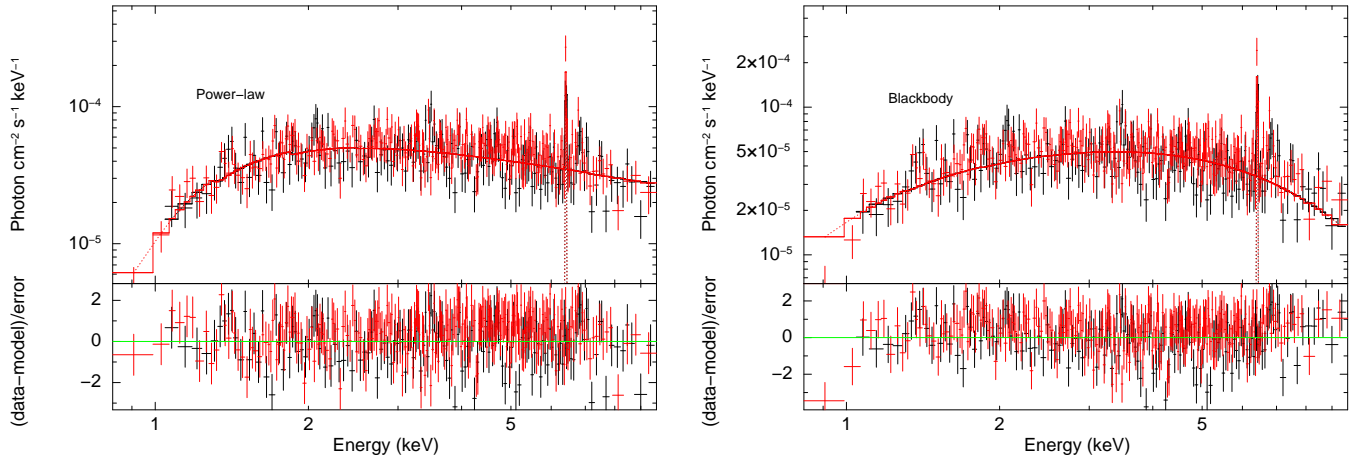


Figure 3. Merged spectra of *XMM-Newton* MOS (black) and pn (red) fitted using an absorbed and *power-law* model (left) or *blackbody* model (right) with a Gaussian line at 6.4 keV. The fit results are shown in Table 2 .

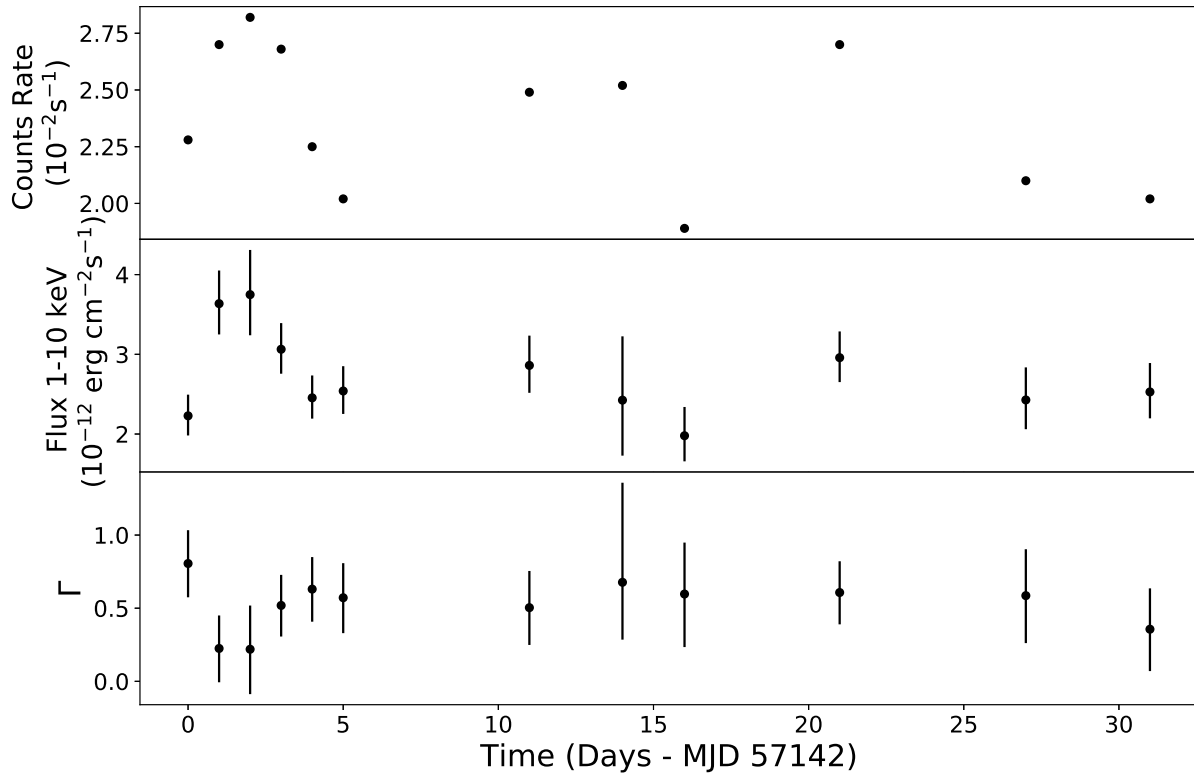


Figure 4. Variation of the counts rate, X-ray flux and spectral index Γ of the 12 *Swift* data taken in 2015.

In order to obtain an overall properties of 3XMM J181923.7–170616, first we produce two merged spectra of *XMM-Newton* (MOS1+2 and pn) by combining the long-time data of each instrument. As shown in the left panel of Figure 3, the spectra can be well described by an absorbed *power-law* model with a photon index of $\Gamma = 0.58 \pm 0.07$ plus a Gaussian line at ~ 6.4 keV ($\chi^2_\nu = 1.11$). The Tübingen-Boulder interstellar medium absorption model *tbabs* is used for calculating the foreground absorption N_{H} and the solar abundances are adopted from Asplund et al. (2009). The best-fit

Table 2. Spectral fit results of the *XMM-Newton* observations

Model 1: <i>power-law</i>					
Year	$\chi^2_\nu/d.o.f.$	N_{H} (10^{22} cm^{-2})	Γ	Fe norm ^a ($10^{-6} \text{ cm}^{-2} \text{ s}^{-1}$)	Flux (1–10 keV) ($10^{-12} \text{ erg cm}^{-2} \text{ s}^{-1}$)
Merged	1.11/404	$1.32^{+0.16}_{-0.15}$	$0.58^{+0.07}_{-0.07}$	$5.83^{+1.92}_{-1.92}$	2.81 ± 0.06
2006	0.99/116	$1.63^{+0.50}_{-0.46}$	$0.59^{+0.19}_{-0.18}$	–	2.83 ± 0.21
2010	1.13/423	$1.34^{+0.24}_{-0.21}$	$0.59^{+0.24}_{-0.21}$	$6.57^{+2.64}_{-2.63}$	2.69 ± 0.13
2013	0.90/91	$1.11^{+0.46}_{-0.42}$	$0.44^{+0.19}_{-0.18}$	–	$3.44^{+0.29}_{-0.27}$
Model 2: <i>blackbody</i>					
Year	$\chi^2_\nu/d.o.f.$	N_{H} (10^{22} cm^{-2})	kT (keV)	Fe norm ^a ($10^{-6} \text{ cm}^{-2} \text{ s}^{-1}$)	Flux (1–10 keV) ($10^{-12} \text{ erg cm}^{-2} \text{ s}^{-1}$)
Merged	1.20/402	0.33 ± 0.09	$2.04^{+0.09}_{-0.08}$	$6.11^{+1.9}_{-1.9}$	2.48 ± 0.09
2006	0.97/116	$0.27^{+0.38}_{-0.27}$	$2.06^{+0.24}_{-0.20}$	$7.73^{+4.63}_{-4.61}$	$2.44^{+0.19}_{-0.20}$
2010	1.17/423	0.33(fixed)	$2.10^{+0.08}_{-0.08}$	$1.92^{+1.20}_{-1.20}$	$2.56^{+0.10}_{-0.10}$
2013	0.92/91	0.33(fixed)	$2.13^{+0.20}_{-0.17}$	–	$2.98^{+0.26}_{-0.25}$

NOTE—The errors are estimated at the 90% confidence level.

^a The flux of Fe line at 6.4 keV in 10^{-6} photons $\text{cm}^{-2} \text{ s}^{-1}$. The value is fixed to 0 and denoted with “–” when it can not be constrained.

foreground absorption N_{H} is $1.32^{+0.16}_{-0.15} \times 10^{22} \text{ cm}^{-2}$ (see spectral results in Table 2) obtained using merged *XMM-Newton* spectra. Although the fit can be slightly improved ($\chi^2_\nu = 1.10$) after adding a Gaussian line at 6.7 keV, the line is too faint to be well constrained and is not clear in individual spectra. Therefore, we only include the 6.4 keV iron $K\alpha$ emission for spectral fit. We also model the spectra with an absorbed *blackbody* model plus a 6.4 keV line, which gives an best-fit absorption of $N_{\text{H}} = 0.33 \pm 0.09 \times 10^{22} \text{ cm}^{-2}$ and a temperature of $kT = 2.04^{+0.09}_{-0.08}$ keV. The *blackbody* fit results in a $\chi^2_\nu = 1.20$ slightly larger than the *power-law* fit and displays large residuals < 1 keV and > 7 keV (see the right panel of Figure 3). Other models, such as *bremsstrahlung* and *diskbb*, are tried but do not provide acceptable fit.

We subsequently model the spectra in each year to investigate the spectral evolution. The *XMM-Newton* spectra in each year are jointly fitted (MOS1, MOS2 and pn). We fit the spectra with the absorbed *power-law/blackbody* models plus a 6.4 keV Gaussian line and show the best-fit results in Table 2. The *power-law* model generally provides a better fit than the *blackbody* model, especially for describing the low-energy spectra. The variation of N_{H} can not be well constrained with the currently available data. The X-ray flux in 1–10 keV was $2.83 \pm 0.21 \times 10^{-12} \text{ erg cm}^{-2} \text{ s}^{-1}$ in 2006, and was not significantly changed in 2010. The observation in 2013 was subject to flaring and we cannot further validate the nature of the flux change. A short-term spectral variation was revealed from the 12 *Swift* observation in 2015, with the 1–10 keV flux increased by $1.52^{+0.5}_{-0.6} \times 10^{-12} \text{ erg cm}^{-2} \text{ s}^{-1}$ within 2 days (MJD 57142–57143; see Figure 4). The flux varied between $2.20 \pm 0.14 \times 10^{-12} \text{ erg cm}^{-2} \text{ s}^{-1}$ and $3.75^{+0.56}_{-0.51} \times 10^{-12} \text{ erg cm}^{-2} \text{ s}^{-1}$, with a hardening as the flux increased.

We also perform a phase-resolved spectroscopic analysis of the *XMM-Newton* spectra. We divide the source time series of the *XMM-Newton* data into four individual phases: -0.2 – 0.2 (valley), 0.2 – 0.4 , 0.4 – 0.6 (peak), 0.6 – 0.8 phases (see Figure 5). We apply the absorbed *power-law/blackbody* models to jointly fit the spectra in the four phases (MOS 1 and MO2 are merged). The fit results are shown in Table 3.

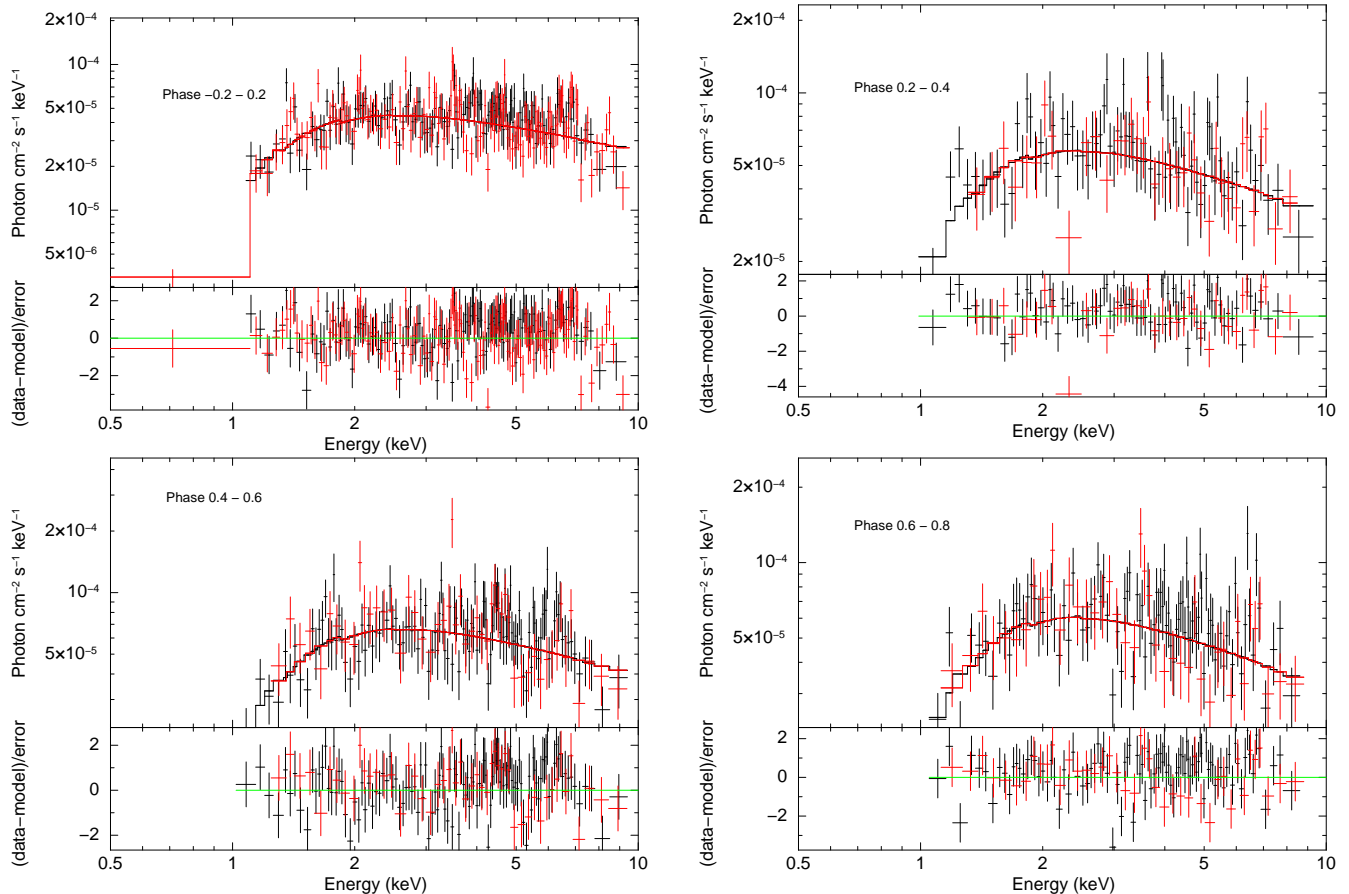


Figure 5. Phase-resolved spectra of *XMM-Newton* MOS (black) and pn (red) data fitted using an absorbed *power-law* model. The fit results are shown in Table 3.

The absorbed *power-law* model can best describe ($\chi^2_\nu \lesssim 1.2$) the spectra of all phases (see Figure 5), with an average column density of $N_{\text{H}} \sim 1.2$ – $1.3 \times 10^{22} \text{ cm}^{-2}$ and a photon index $\Gamma \sim 0.6$. Since the absorption value of phase 0.6 – 0.8 can not be constrained under the *blackbody* model, we fix this value to the N_{H} result of the merged spectra. The table shows that among the phases there is little change to the parameters other than the flux. We have also examined the Fe $K\alpha$ emission line flux in each phase, and have not found a significant change of the Fe line flux. Hereafter, we adopt the *power-law* results as they best describe the spectra.

4. DISCUSSION

We have shown that 3XMM J181923.7–170616 is a pulsating X-ray source with a period of $407.904(7) \text{ s}$ and a spin down rate of $5.9 \pm 5.4 \times 10^{-9} \text{ ss}^{-1}$. The spectra is best characterized

Table 3. Results of the phase resolved spectroscopy with the *XMM-Newton* data

Model 1: <i>power-law</i>				
Phase	$\chi^2_\nu/d.o.f.$	N_{H} (10^{22} cm^{-2})	Γ	Flux(1-10 keV) ($10^{-12} \text{ erg cm}^{-2}\text{s}^{-1}$)
-0.2 – 0.2	1.22/269	$1.25^{+0.24}_{-0.23}$	$0.55^{+0.10}_{-0.10}$	2.56 ± 0.11
0.2 – 0.4	1.14/115	$1.18^{+0.37}_{-0.32}$	$0.59^{+0.16}_{-0.16}$	$3.17^{+0.22}_{-0.23}$
0.4 – 0.6	1.15/173	$1.29^{+0.30}_{-0.27}$	$0.53^{+0.13}_{-0.13}$	$3.88^{+0.21}_{-0.22}$
0.6 – 0.8	1.17/137	$1.21^{+0.31}_{-0.30}$	$0.62^{+0.16}_{-0.15}$	$3.27^{+0.23}_{-0.21}$
Model 2: <i>blackbody</i>				
Phase	$\chi^2_\nu/d.o.f.$	N_{H} (10^{22} cm^{-2})	kT (keV)	Flux(1-10 keV) ($10^{-12} \text{ erg cm}^{-2}\text{s}^{-1}$)
-0.2 – 0.2	1.30/269	0.33(fixed)	$2.15^{+0.10}_{-0.09}$	$2.30^{+0.10}_{-0.08}$
0.2 – 0.4	1.20/115	$0.14^{+0.22}_{-0.14}$	2.0 ± 0.2	$2.74^{+0.21}_{-0.23}$
0.4 – 0.6	1.18/173	$0.17^{+0.18}_{-0.17}$	2.2 ± 0.2	$3.47^{+0.21}_{-0.22}$
0.6 – 0.8	1.30/137	0.33 (fixed)	1.9 ± 0.1	$2.78^{+0.20}_{-0.19}$

NOTE—The errors are estimated at the 90% confidence level.

with a hard power-law with Fe lines at 6.4 keV and 6.7 keV. The flux in 1–10 keV has varied between $2\text{--}4 \times 10^{-12} \text{ erg cm}^{-2} \text{ s}^{-1}$, and spectral index Γ was in the range of 0.2–0.8. It appears to be a persistent source without luminous burst detected during the observation epochs. The absorption column density $N_{\text{H}} = 1.32^{+0.16}_{-0.15} \times 10^{22} \text{ cm}^{-2}$ determined by XMM observations is similar to the value of the Galactic hydrogen column density $\sim 1.2\text{--}1.3 \times 10^{22} \text{ cm}^{-2}$ in this direction (Willingale et al. 2013). It implies that the X-ray source is distant and possibly located near the boundary of the Galactic plane. We conservatively set the lower limit of the distance of the X-ray source to the rotation tangent position at ~ 8 kpc. Hereafter the distance is parameterized as $10d_{10}$ kpc, given that the interstellar gas distribution along the line of sight is uncertain.

4.1. Search for optical and near-infrared counterpart

We searched in the archival data and catalogues for the optical and near-IR counterparts of 3XMM J181923.7–170616. The 1σ positional uncertainty for 90% of the point sources in the 3XMM catalog is $2''.4$.

Using the VizieR catalogue access tool (Ochsenbein et al. 2000), we found a faint optical source (source #1; $18^{\text{h}}19^{\text{m}}23^{\text{s}}73$, $-17^{\circ}06'16''.10$, J2000) with the apparent magnitudes $M_R = 20.90 \pm 0.09$ and $M_I = 19.22 \pm 0.04$ in the VPHAS+ DR2 point source catalog (Drew et al. 2014, 2016), which is $0''.5$ away from 3XMM J181923.7–170616. It also shows an $\text{H}\alpha$ line with a magnitude of 20.5 ± 0.2 . The optical source spatially matches a near-IR source ($M_J = 16.758 \pm 0.018$, $M_H = 15.939 \pm 0.019$, and $M_K = 15.320 \pm 0.026$), recorded in the UKIDSS Galactic Plane Survey (Lucas et al. 2012). We also notice that it matches the source PSO J181923.731-170616.083 in the Panoramic Survey Telescope

and Rapid Response System (Pan-STARRS) survey (Chambers et al. 2016). Source #1 was detected in the r,i,z,y bands among the five filter bands used in the Pan-STARRS survey. Figure 6 shows the I-band image of the optical source. In Figure 7, we show the spectral energy distribution (SED) of source #1. It includes photometry in the bands mentioned above. We fit the SED with an absorbed blackbody model, while the absorbed power-law model can not explain the convex spectra. The V-band absorption A_V of 4.7 is converted from the foreground absorption $N_H = 1.35 \times 10^{22} \text{ cm}^{-2}$ using a conversion factor $N_H = 2.87 \times 10^{21} A_V \text{ cm}^{-2}$ (Foight et al. 2016). The ratio of total to selective extinction at V band $R_V = 3.1$ is adopted for the calculation of the absorption at each wavelength. The fit shows that source #1 has an effective temperature of $T_{\text{eff}} = 4226 \pm 151 \text{ K}$ and luminosity of $4.7 \pm 0.2 \times 10^{34} d_{10}^2 \text{ erg s}^{-1}$. The temperature and luminosity of source #1 is similar to a giant star with a spectral type of K3 III.

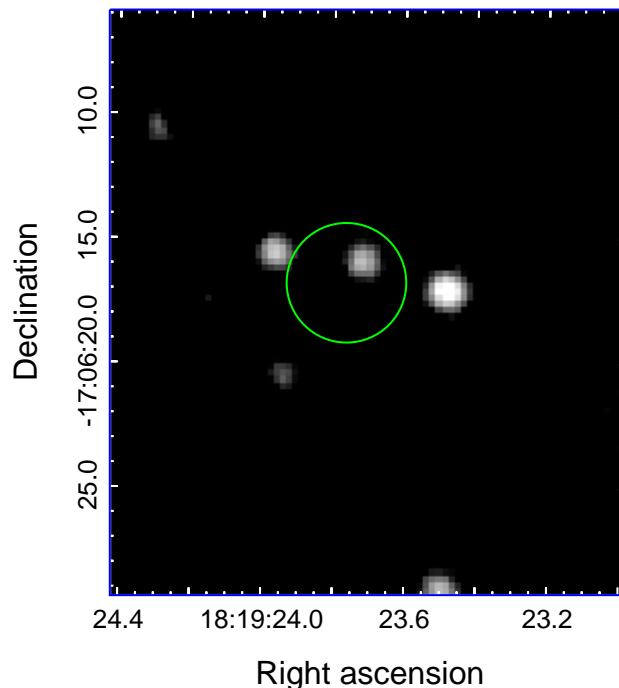


Figure 6. I-band image obtained from the Pan-STARRS DR1 Archive. The green circle indicates the location of 3XMM J181923.7–170616 and its 1σ uncertainty radius of $2''.4$.

There is another near-IR UKIDSS source located $\sim 2''$ away (source #2; $18^{\text{h}}19^{\text{m}}23^{\text{s}}.76$, $-17^{\circ}06'17''.67$, J2000) with $M_J = 17.497 \pm 0.035$, $M_H = 15.547 \pm 0.014$, and $M_K = 14.622 \pm 0.014$, which might be the same source with $M_{3.6\mu\text{m}} = 13.5 \pm 0.1$, $M_{4.5\mu\text{m}} = 13.76 \pm 0.30$, and $M_{5.8\mu\text{m}} = 12.34 \pm 0.29$ in the GLIMPSE source catalog. The blackbody fit shows that source #2 has a temperature of $\sim 1880 \text{ K}$ and luminosity of $3.5 \times 10^{34} d_{10}^2 \text{ erg s}^{-1}$.

The spectra of source #1 and #2 are not compatible with OB supergiants ($10^4 L_{\odot}$) or hot main-sequence stars ($T_{\text{eff}} > 10^4 \text{ K}$). Nevertheless, we can not exclude the possibility that the donor star of 3XMM J181923.7–170616 is a Be and the emission of the stellar component was not detected with current surveys. Some Be stars exhibit IR excess with a blackbody temperature of thousands of kelvin, which is attributed to the circumstellar material (Zhang et al. 2005). Assuming a detection limit of 21 magnitude in V band, current surveys may fail to detect a star with an absolute magnitude

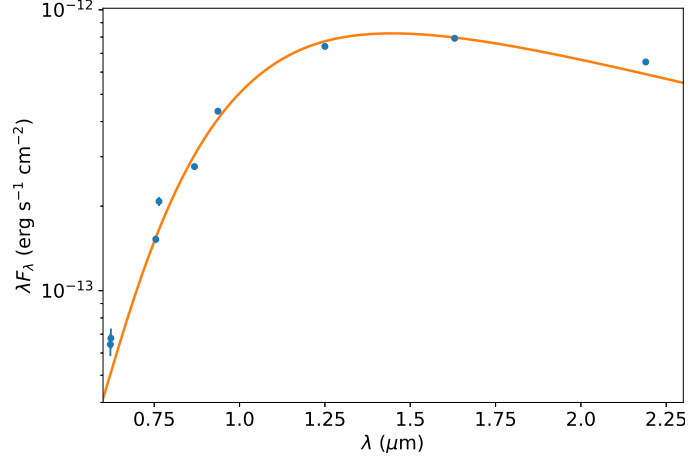


Figure 7. Spectral energy distribution of source #1 (dots with error bars) fitted with an absorbed blackbody model ($A_V = 4.7$, $T_{\text{eff}} = 4226$ K and $L = 4.7 \times 10^{34} d_{10}^2$ erg s $^{-1}$).

> -1.1 at an assumed distance of 30 kpc (near Galactic edge; $A_V = 4.7$), which corresponds to a main-sequence star no earlier than B3-type. It is also unclear whether the two IR sources are relevant or only foreground/background sources projected near 3XMM J181923.7–170616. Further targeted optical and IR observations are needed to achieve a firm conclusion.

The position accuracy of 3XMM J181923.7–170616 can be improved by performing an astrometric analysis with the Swift-XRT data products generator³. The position coordinates are derived from the XRT data product detecting and localizing all sources in the image, and then matching them with the 2MASS catalogue sources (Evans et al. 2014). This substantially increases the position accuracy to a 90% confidence error radius of $0''.6$ centered at $18^{\text{h}}19^{\text{m}}23^{\text{s}}.73$, $-17^{\circ}06'15''.9$, which is consistent with the position of the optical–IR source #1.

4.2. The nature of 3XMM J181923.7–170616

3XMM J181923.7–170616 was considered to be a candidate of a slowly spinning X-ray pulsar (Farrell et al. 2015) and its nature remained unclear. Based on the analysis described above, we here discuss three possible scenarios for the nature of the X-ray source: an isolated NS, a cataclysmic variable (CV) or an X-ray binary.

If 3XMM J181923.7–170616 is an isolated NS, the long period and the period derivative would suggest a rotational energy loss $\dot{E}_{\text{rot}} = 3.95 \times 10^{46} P^{-3} \dot{P} \leq 3.4 \pm 3.1 \times 10^{30}$ erg s $^{-1}$, which is insufficient to power the observed X-ray emission ($L_X = 2.78 \times 10^{34} d_{10}^2$ erg s $^{-1}$). In this case, the long period and low \dot{E}_{rot} would suggest that the source is not a classical rotation powered NS, but may be a magnetar. Magnetars are NSs with ultra-strong magnetic fields and their X-ray emission is powered by the decay of the magnetic fields (Thompson & Duncan 1995, 1996; Thompson et al. 2002). The known magnetars have periods 2–12 s, except one candidate 1E 161348–5055 in the supernova remnant RCW 103 showing surprisingly large period of 6.67 hr (De Luca et al. 2006). Besides the anomalous long period, the X-ray emission of 3XMM J181923.7–170616 appears to be much more stable than magnetars undergoing outbursts, when the magnetars are up to 10^3 times brighter than the steady state and then experience a decay lasting a few weeks to months (Rea & Esposito 2011).

³ http://www.swift.ac.uk/user_objects/

It also can not be a quiescent magnetar, since the quiescent X-ray emission of a magnetar is soft according to the magneto-thermal evolution model (Viganò et al. 2013) and observations (a power-law photon index = 1.5-4 or blackbody temperature $kT_{BB} = 0.1-0.7$ keV; Olausen & Kaspi 2014). Moreover, the iron line at 6.4 keV supports the existence of cold materials surrounding the source. Therefore, the isolated pulsar explanation is not favored according to the spectral behaviors.

3XMM J181923.7–170616 is more luminous than CVs which have a typical luminosity $L_X \lesssim 10^{34}$ erg s⁻¹ (Burenin et al. 2016). CVs show blackbody radiation during the outburst state (Mukai et al. 2003), while in quiescent state the emission becomes optically thin and presents multi-temperature Bremsstrahlung radiation (Mukai 2001, Richman et al. 1996, Bernardini et al. 2012). The X-ray emission of 3XMM J181923.7–170616 does not show significant variation and the spectra cannot be well fitted with an optically thin model, making the CV explanation unlikely.

The remaining possibility is an X-ray binary. Since only one periodicity has been found with the *Swift* and *XMM-Newton* data, we need to discuss whether the 408 s is a spin period or an orbital period. According to the Kepler’s third law, the orbital period P_{orb} depends on the masses of the primary (M_X) and the donor (M_*), and the separation between them (a): $P_{\text{orb}} = 2\pi a^{3/2}/[G(M_X + M_*)]^{1/2}$. Assuming $P_{\text{orb}} = 408$ s and $M_X = 1.4 M_\odot$ for an NS, the separation a are obtained as $0.16R_\odot$ and $0.27R_\odot$, respectively (for a donor mass of $1 M_\odot$ and $10 M_\odot$, where R_\odot is the solar radius). If the 408 s is an orbital period, the companion radius must be much smaller than solar radius (e.g., a degenerate companion), and the X-ray source could be a ultra-compact LMXB with the smallest known P_{orb} among its group. However, the hard spectra ($\Gamma < 1$ or $kT \sim 2$ keV) are atypical for those low-level accretion LMXBs ($L_X \sim 10^{34-36}$ erg s⁻¹ and $\Gamma \gtrsim 1.4$; e.g., Wijnands et al. 2015; in’t Zand et al. 2005; Wijnands et al. 2006) or for those in the quiescent (temperature of less than a few hundred eV; $L_X = 10^{30-33}$ erg s⁻¹; e.g., Heinke et al. 2003). Therefore, we suggest the 408 s is the pulsar spin period.

The long spin period and hard X-ray spectra widely exist in HMXBs. The hard power-law emission can be interpreted as Comptonization of the thermal photons by the high-energy electrons. 3XMM J181923.7–170616 is unlikely to be a SGXB due to the absence of OB supergiant at its location (see Section 4.1). The X-ray properties of the source indeed well matches the characteristics of persistent Be X-ray binaries, including the long pulse period ($P_{\text{spin}} \gtrsim 200$ s), persistent and low-luminosity ($\leq 10^{34-35}$ erg s⁻¹), low X-ray variability and hard spectrum with faint Fe 6.4 keV line (Reig & Roche 1999; Reig 2011). In this case, the NS is orbiting in a low-density region of the Be star’s wind. This explanation is waiting to be tested, given that no massive star earlier than B3 has been detected at the position of 3XMM J181923.7–170616.

SyXBs are a new group of XRBs that display some X-ray properties similar to HMXBs but are systems that host a K/M-type giant as its donor. These objects display long pulse periods ($\gtrsim 100$ s), low luminosity, and hard power-law spectra (0.5–2; Enoto et al. 2014). As mentioned in Section 4.1, an optical/IR source spatially consistent 3XMM J181923.7–170616 shows characteristics of an K3 giant. The SyXBs scenario is therefore most favorable nature of 3XMM J181923.7–170616 due to the existence of a late type counterpart candidate.

Hence, 3XMM J181923.7–170616 is most likely an SyXB with a K-type giant donor (source #1, see Figure 6). An alternative possibility is that it is a persistent BeXB with a companion star no earlier than B3. Future X-ray and optical monitoring observations will shed light on the other period and the type of the companion star, so as to confirm the nature of 3XMM J181923.7–170616.

5. SUMMARY

We have performed a detailed X-ray analysis of 3XMM J181923.7–170616 using the *XMM-Newton* and *Swift* observations spanning over 9 years. The main conclusions are the following:

1. We have accurately determined the spin period of $P = 407.904(7)$ s and discovered the spinning down of the source with $\dot{P} \leq 5.9 \pm 5.4 \times 10^{-9} \text{ s s}^{-1}$ (1σ). The pulse shape is similar to a sinusoid profile and does show significant change in 9 yrs.
2. 3XMM J181923.7–170616 emits persistent X-ray emission which is best characterized by an absorbed power-law emission with $N_{\text{H}} \sim 1.32 \times 10^{22} \text{ cm}^{-2}$ and $\Gamma \sim 0.6$ plus two Fe lines at 6.4 keV and 6.7 keV. The source experienced a small flux variation ($2\text{--}4 \times 10^{-12} \text{ erg cm}^{-3} \text{ s}^{-1}$), with a spectral hardening as the flux increased. No burst activities have been observed during the observation epochs. We performed phase-resolved spectroscopy and do not find significant change of N_{H} , Γ and the flux of 6.4 keV line between different phases.
3. The absorption column density of 3XMM J181923.7–170616 is similar to the total Galactic N_{H} along its direction, indicating that it is a distant source. We searched for optical and IR counterparts from the archival surveys, and exclude the existence of a Galactic OB supergiant. We discover an optical counterpart with a temperature and luminosity similar to a K3-type giant.
4. We discussed the nature of 3XMM J181923.7–170616 by comparing its properties with those of isolated NSs, CVs and X-ray binaries. It is unlikely to be an isolated magnetar, given the relatively small variability, hard spectra, and the existence of surrounding cold materials as indicated by the 6.4 keV line. The luminosity and the spectra are also not consistent with the properties of a CV. An X-ray binary is the probable explanation. An SyXB is the favored nature of 3XMM J181923.7–170616 and can essentially explain its low luminosity, slow pulsation, hard spectrum, and possible late type companion. An alternative explanation of the source is a persistent Be/X-ray binary with a companion star no earlier than B3-type.

We acknowledge the anonymous referee for suggestions regarding the phase-connection analysis and the position accuracy. We thank Peng Wei and Eugene Magnier for helpful discussion about the search of the optical/IR counterpart. This work was supported by NSFC grants 11503008 and J1210039, and Top-notch Academic Programs Project of Jiangsu Higher Education Institutions. P.Z. acknowledges the support from the NWO Veni Fellowship, grant no. 639.041.647, and NSFC grant 11233001. W.Y. was supported in part by the NSFC grant no. 11333005 and by the National Program on Key Research and Development Project (grant no. 2016YFA0400804). X.L. was supported by the National Program on Key Research and Development Project (grant no. 2016YFA0400803), and the NSFC grants 11133001 and 11333004. X.X. thanks the support by NSFC grant 11303015.

REFERENCES

- | | |
|---|--|
| Asplund, M., Grevesse, N., Sauval, A. J., & Scott,
P. 2009, <i>ARA&A</i> , 47, 481 | Bernardini, F., de Martino, D., Falanga, M., et al.
2012, <i>A&A</i> , 542, A22 |
|---|--|

- Burenin, R. A., Revnivtsev, M. G., Tkachenko, A. Y., et al. 2016, *Astronomy Letters*, 42, 240
- Chambers, K. C., Magnier, E. A., Metcalfe, N., et al. 2016, arXiv:1612.05560
- De Luca, A., Caraveo, P. A., Mereghetti, S., Tiengo, A., & Bignami, G. F. 2006, *Science*, 313, 814
- Drew, J. E., Gonzalez-Solares, E., Greimel, R., et al. 2014, *MNRAS*, 440, 2036
- Drew, J. E., Gonzalez-Solares, E., Greimel, R., et al. 2016, *VizieR Online Data Catalog*, 2341, <http://adsabs.harvard.edu/abs/2016yCat.2341....0D>
- Edwards, R. T., Hobbs, G. B., & Manchester, R. N. 2006, *MNRAS*, 372, 1549
- Enoto, T., Sasano, M., Yamada, S., et al. 2014, *ApJ*, 786, 127
- Evans, P. A., Osborne, J. P., Beardmore, A. P., et al. 2014, *ApJS*, 210, 8
- Farrell, S. A., Murphy, T., & Lo, K. K. 2015, *ApJ*, 813, 28
- Foight, D. R., Güver, T., Özel, F., & Slane, P. O. 2016, *ApJ*, 826, 66
- Heinke, C. O., Grindlay, J. E., Lugger, P. M., et al. 2003, *ApJ*, 598, 501
- Hobbs, G. B., Edwards, R. T., & Manchester, R. N. 2006, *MNRAS*, 369, 655
- in't Zand, J. J. M. 2005, *A&A*, 441, L1
- Leahy, D. A. 1987, *A&A*, 180, 275
- Lü, G.-L., Zhu, C.-H., Postnov, K. A., et al. 2012, *MNRAS*, 424, 2265
- Mukai, K., Kinkhabwala, A., Peterson, J. R., Kahn, S. M., & Paerels, F. 2003, *ApJL*, 586, L77
- Mukai, K. 2001, arXiv:astro-ph/0112048
- Negueruela, I. 1998, *A&A*, 338, 505
- Ochsenbein, F., Bauer, P., & Marcout, J. 2000, *A&AS*, 143, 23
- Olausen, S. A., & Kaspi, V. M. 2014, *ApJS*, 212, 6
- Rea, N., & Esposito, P. 2011, *Astrophysics and Space Science Proceedings*, 21, 247
- Reig, P. 2011, *Ap&SS*, 332, 1
- Reig, P., & Roche, P. 1999, *MNRAS*, 306, 100
- Richman, H. R. 1996, *ApJ*, 462, 404
- Rosen, S. R., Webb, N. A., Watson, M. G., et al. 2016, *A&A*, 590, A1
- Strüder, L., Briel, U., Dennerl, K., et al. 2001, *A&A*, 365, L18
- Thompson, C., Lyutikov, M., & Kulkarni, S. R. 2002, *ApJ*, 574, 332
- Thompson, C., & Duncan, R. C. 1995, *MNRAS*, 275, 255
- Turner, M. J. L., Abbey, A., Arnaud, M., et al. 2001, *A&A*, 365, L27
- UKIDSS Consortium 2012, *VizieR Online Data Catalog*, 2316,
- Viganò, D., Rea, N., Pons, J. A., et al. 2013, *MNRAS*, 434, 123
- Wijnands, R., Degenaar, N., Armas Padilla, M., et al. 2015, *MNRAS*, 454, 1371
- Wijnands, R., in't Zand, J. J. M., Rupen, M., et al. 2006, *A&A*, 449, 1117
- Willingale, R., Starling, R. L. C., Beardmore, A. P., Tanvir, N. R., & O'Brien, P. T. 2013, *MNRAS*, 431, 394
- Zhang, P., Chen, P. S., & Yang, H. T. 2005, *NewA*, 10, 325